Analysis of Rotational Column with Plastic Hinge

Michael Long, Rice University;   Corey Bergad, Bates College;
EERC Name: MCEER
Host Institution: SUNY at Buffalo
Faculty Advisor: Dr. Andrei Reinhorn

Abstract: A plastic hinge is a type of energy dampening device allowing plastic rotation of an otherwise rigid column connection. This device is composed of a weakened portion of the column prevented from rotating by relatively small steel members. These small bars are designed to yield and allow rotation before the capacity of the column is reached, thus acting as mechanical fuses protecting the column from fatigue. After a seismic event the fuse bars can be easily replaced, restoring the column to its original condition. To function properly the hinge must become plastic before the column above it yields, but limiting the deflection at the top of the column is also desirable for the stability of the overlying structure, necessitating a hinge with some degree of strength.   The experimental setup of this study was constructed in the University at Buffalo's Structural Engineering and Earthquake Simulation Laboratory in 2004 and was comprised of a steel column subjected to lateral displacement at the top with a plastic hinge fixed at the base, simulating earthquake-induced ground motion on a bridge column. The purpose of this research was to develop an accurate model of the column-hinge system in the elastic range of the fuse bars, allowing consideration of the above design criteria for later testing. Plastic behavior of the fuse bars was not tested. Experimental data was generated using a quasi-static cyclic loading pattern.   The behavior of the system was shown to be in agreement with the analytical model.

Introduction

Plastic hinges are an extension of the ductile design concept in building seismically resistant structures. Energy is dissipated through the plastic deformation of specific zones at the end of a member without collapsing the rest of the structure. In conventional reinforced concrete columns, this plastic hinge action can result in damage and permanent strain in the column, necessitating replacement of the entire member and possibly the entire structure. However, through the use of specially designed plastic hinge zones, damage due to large seismic displacements can be localized and repaired after an earthquake. This design philosophy was termed Control and Repairability Damage (CARD) by Cheng and Mander (1997).

In reinforced concrete columns, the detailed plastic hinge consists of a weakened portion of the column near the top and bottom where the longitudinal reinforcement is decreased, allowing yielding in this zone before the rest of the column is damaged. These specially weakened steel bars are termed fuse-bars since they are designed to yield and thus protect the rest of the column during repeated ground motion. Fuse-bars are attached so as to be easily replaced, restoring the column to its original condition. The practicality

and effectiveness of this method was demonstrated in the work of Cheng and Mander (1997).

The column used for this study was designed using a similar concept meant to simulate an earthquake-induced deflection on a bridge column. The experimental setup, shown in Figure 1, consisted of an S3x5.7 steel member subjected to lateral displacement at the top applied by a hydraulic actuator, while remaining fixed at its base to a specially designed plastic hinge. A pinned connection at both actuator mounts ensured that the actuator applied no axial force on the column. The plastic hinge, detailed in Figure 2, consisted of a pinned connection between the column and load cell at the base, which is in turn bolted to the reaction frame. The pin is surrounded by four small, vertical steel members preventing rotation and acting as fuse-bars. These bars were threaded into place and held by hand-tightened nuts, thus making them easily replaceable. The fuse-bars themselves are 5" sections of 1/2" threaded 100 ksi stainless steel. There is a 2" section in the middle of these bars where the threads have been removed and the diameter is 3/8".
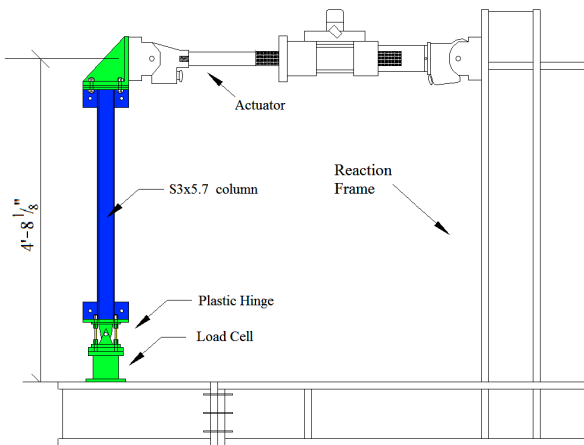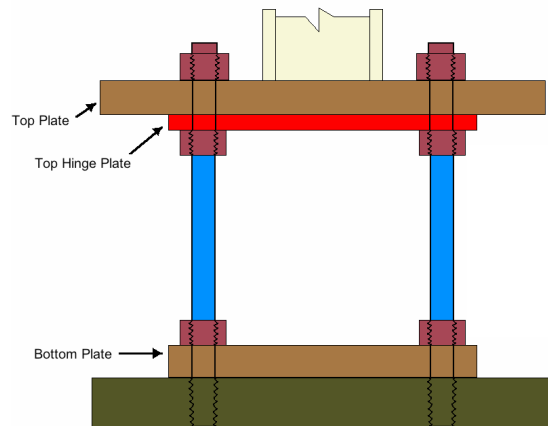

Figure 1: Overall Experimental setup

Figure 2: Detail of Hinge

The objective of this research was to analytically model the behavior of this specific rotational column, and then compare the model to experimental observations. The model could then be used by other researchers to appropriately design the strength of the plastic hinge and run a displacement-controlled test pattern on the column which would yield the hinge, but not damage the column. Therefore, both a stress and deflection analysis of the column-hinge setup was required. Only an elastic analysis of the hinge was made; the fuse-bars were not yielded during experimentation.
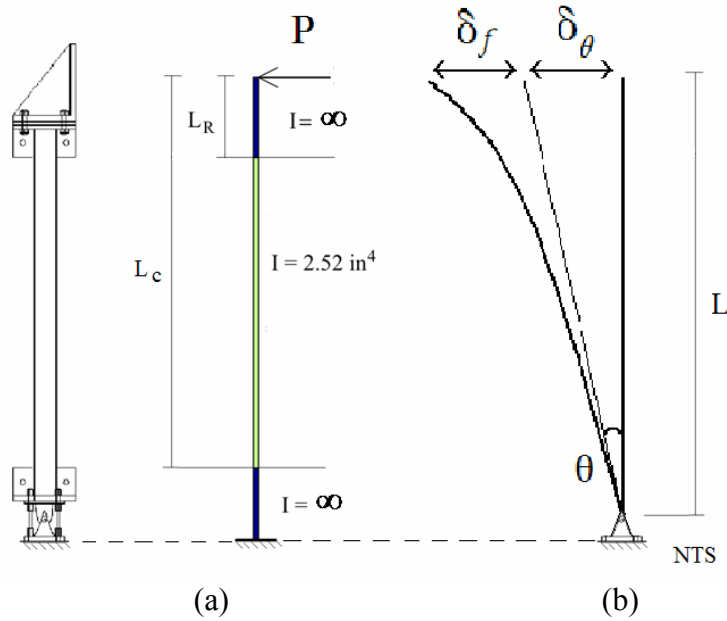
Figure 3: (a) Theoretical model of flexural stiffness and (b) Deflection due to rotation of hinge and flexure of S3x5.7 member

Analytical Model

A load P imposed by the actuator acting at a distance L from the pin results in deflection due to flexure of the S3x5.7 member, labeled δ_f, and rotation of the pinned connection at the base by some angle θ, labeled δ_θ. These deflections can be independently calculated and then combined using theoretical stiffness coefficients for rotation of the pin and flexure of the beam:

$$\delta_\theta = \theta \times L = \frac{PL^2}{K_\theta} \qquad\qquad \text{Eq. (1)}$$

$$\delta_{flex} = \frac{P}{K_{flex}} \qquad\qquad \text{Eq. (2)}$$

where PL = moment acting on the hinge; K_θ = angular stiffness of the hinge; and K_{flex} = flexural stiffness of the column.

The flexural stiffness of the column was determined using the assumption that all connecting plates and the widened portion of the steel member were rigid (i.e. $I = \infty$), as illustrated in Figure 3(a). Flexure would then only occur in the S3x5.7 member. Treating it as a cantilever with a rigid extension at the end allowed the derivation of a simple formula for flexural deflection:

$$\delta_{flex} = \frac{PL_c^3}{3EI_c}\left[1 - \left(\frac{L_R}{L_c}\right)^3\right] \qquad\qquad \text{Eq. (3)}$$

where Lc = free length of the S3x5.7 column plus the rigid extension on top; LR = length of the rigid connecting portion at the top; E = Young's Modulus for steel; and I $_c$ =

second moment of area for the X-X axis of an S3x5.7 member given by the ASCI manual.

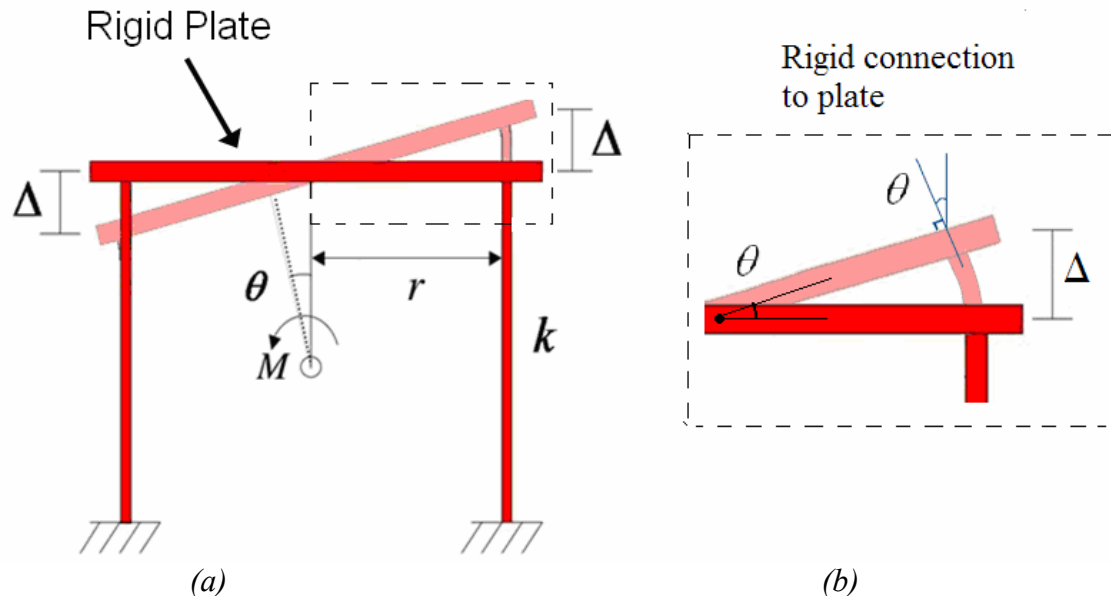*(a)*   *(b)*

Figure 4: (a) Motion of the hinge is due to moment about pin in center. (b) Using small angle theory, rotation of the top plate can be modeled

The stiffness of the hinge is related to the moment acting about the pin in the center. This moment causes rotation of the hinge, resisted by the axial and bending forces within the fuse-bars. Assuming the top plate of the hinge is rigid, axial elongation will be symmetrical for tension and compression, and the end rotation of the fuses will equal the rotation of the pin, denoted by θ. Furthermore, by small angle approximation the axial elongation will be:

$$\Delta = \theta\, r \qquad\qquad\qquad\qquad\qquad\qquad\qquad\qquad \text{Eq. (4)}$$

where r = lateral radius from the pin to the center of the fuse. Multiplying Eq (4) by the axial stiffness k of each fuse will then give the axial force in each fuse.

Although the tip rotation and deflection were symmetric for tension and compression, the deformable length of the fuse-bars was believed to differ for bending, axial tension, and axial compression. This discrepancy was corrected by the calculation of an effective length for axial force calculations that modeled the overall behavior of the four-fuse system.
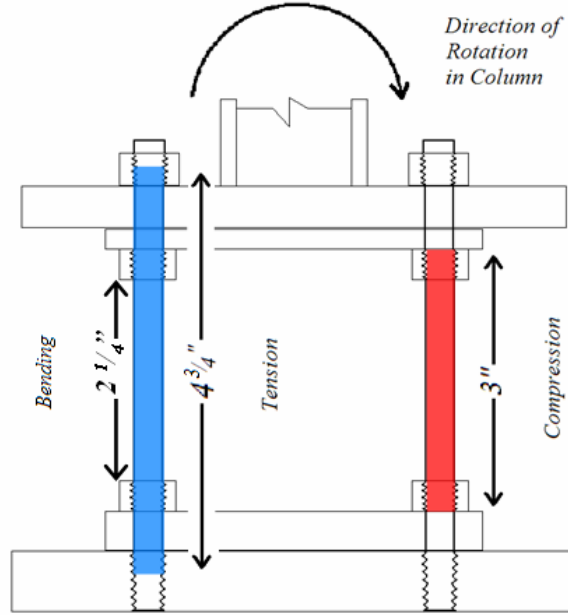
Figure 5: Effective lengths for bending and axial deformations

After solving for the average stiffness, the effective length for axial elongation l_e could be determined and a different value l used for bending calculations:

$$F_{axial} = \frac{EA}{l_e}\theta r \qquad\qquad \text{Eq. (5)}$$

$$M_{bending} = \frac{EI}{l}\theta \qquad\qquad \text{Eq. (6)}$$

where A = cross-sectional area of the fuse and I = second moment of area of the fuse. Any difference in magnitude between the axial force in the tension fuse and the compression fuse was balanced by a vertical force in the pin, not affecting the moment equilibrium about the pin.

A special consideration for the fuse-bar in compression was buckling failure. As shown in Figure 5, bending, and thus buckling, was confined to the portion exposed between the inside nuts; the surrounding material prevents flexural movement in other regions. The critical compression load P_{cr} at which the column will buckle is given by:

$$P_{cr} = \frac{\pi^2 EI}{L_E^{\,2}} \qquad\qquad \text{Eq. (7)}$$

$$L_E = k_E L \qquad\qquad \text{Eq. (8)}$$

where L_E =Euler length for buckling found by multiplying the physical length L by constant k_E. The Euler length used for buckling calculations depends on the boundary conditions of the member, as shown in Figure 6.
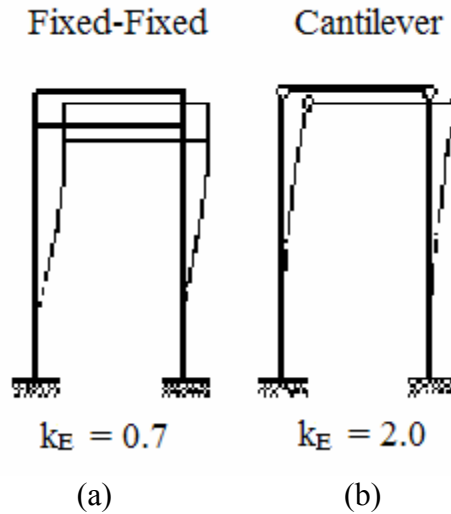
Figure 6: Euler length coefficients for buckling; the two extreme cases for this experiment are shown

The fuse bars weren't free to rotate at their ends, but neither were they completely fixed; a specific end rotation was imposed by the hinge plate. Therefore, the boundary conditions lay somewhere in between the fixed-fixed and cantilever case shown in Figure 6(a) and 6(b), respectively. For axial compression, the failure load is given by:

$$P_{cr} = \sigma_y A \qquad \qquad \text{Eq. (9)}$$

where σ_y = the yielding strength of the steel. Even using the more conservative cantilever case for Eq (8) and a high compressive strength of σ_y= 100 ksi, the critical buckling load given by Eq (7) of 17.4 kips was well above the yielding load of 10 kips given by Eq (9).
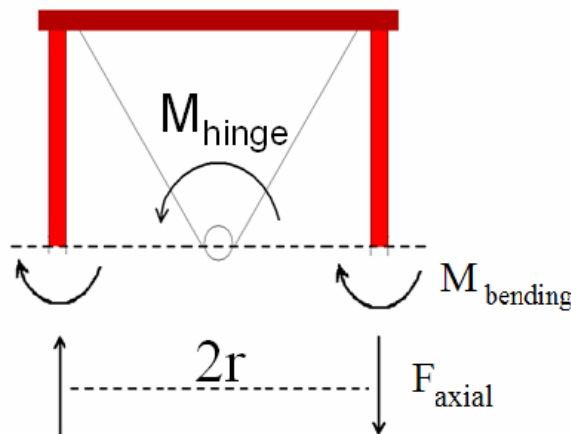

Figure 7: Free body diagram of hinge, illustrating moment equilibrium about pin

As shown in the free body diagram in Figure 7, the moment from an external load M_{hinge} is counteracted by the axial force couple $F_{axial} \times 2r$ and the local bending moment $M_{bending}$ within each fuse. The relationship between these is made clear by summing the moments about the pin for the entire hinge:

$$\Sigma M_{pin} = M_{hinge} - 4(F_{axial} \times r + M_{bending}) = 0 \qquad \text{Eq. (10)}$$

The resultant angular stiffness for the hinge therefore has a bending and an axial component. Using Eq (5) and (6):

$$K_\theta = \frac{M_{hinge}}{\theta} = 4\left(\frac{EAr^2}{l_e} + \frac{EI}{l} \right) \qquad \text{Eq. (11)}$$

Together with the theoretical flexural stiffness given by Eq (3), the deflection of the whole system could now be predicted by adding Eq (1) and (2) for a given load from the actuator.
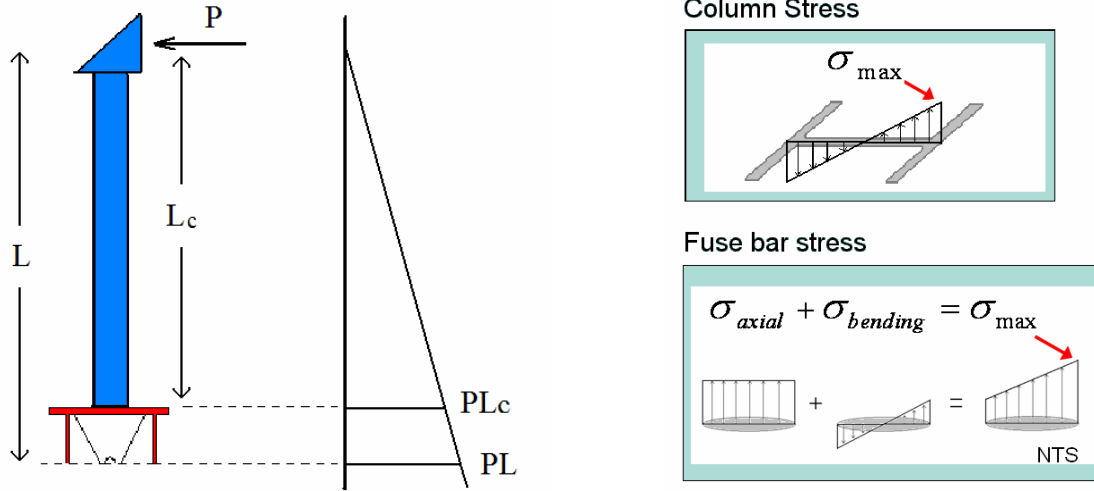

Figure 8: Determination and comparison of maximum stress in the flexural member and the fuse bars

Determining the maximum stress in the different components of the setup was the next step. As shown in Figure 8, the stress in each fuse-bar was a combination of axial and bending stress:

$$\sigma_{axial} = \frac{F_{axial}}{A} = \frac{Er}{l_e} \frac{PL}{K_\theta} \qquad \text{Eq. (12)}$$

$$\sigma_{bending} = \frac{M_{bending}}{S} = \frac{EI}{lS} \frac{PL}{K_\theta} \qquad \text{Eq. (13)}$$

where S is the section modulus of the circular fuse-bars. The maximum stress occurred at the extreme outside fiber of the fuses, where these two stress components act in the same direction. By plugging in Eq (11) for K_θ the stress can be expressed as:

$$\sigma_{fuse} = \sigma_{axial} + \sigma_{bending} = \frac{PL}{4\left(\dfrac{Ar^2}{l_e} + \dfrac{I}{l}\right)}\left(\frac{r}{l_e} + \frac{D}{2l}\right)$$

<div align="right">Eq. (14)</div>

where D = diameter of the circular fuse-bars. This combination related stress to a load applied at the top of the column and controlled the moment capacity of the hinge. Similarly, the moment capacity of the S3x5.7 column at its own point of maximum stress could be related to the actuator load by:

$$\sigma_{column} = \frac{M}{S} = \frac{PL_c}{S_{xx}}$$

<div align="right">Eq. (15)</div>

allowing comparison of stress in the column to stress in each fuse-bar using a common parameter P, the actuator load.

Given a material with a specific yielding strength, Eq (14) shows that the three parameters controlling the moment capacity of the hinge are the fuse-bar's cross-section, radius from the pin, and effective length. For the practical design of this specific setup, cross-sectional area and yielding strength are the only variables which could be altered to raise or lower the moment capacity of the hinge.

As noted previously, Eq (4) made use of small angle assumptions to relate axial elongation of the fuse to rotation of the pin in a simple linear fashion. For comparison, the same relationship for the general case can be expressed as:

$$\Delta = 2\frac{r}{\cos\beta}\sin\left(\frac{\theta}{2}\right)\cos\left(\frac{\theta}{2} + \beta\right)$$

<div align="right">Eq. (16)</div>

where the angle β is a function of hinge geometry. The error associated with this approximation was considered negligible at the displacements involved in the elastic range of the hinge. For illustration, Table 1 shows the error in the Δ calculation, as well as two derived quantities, the deflection and load imposed by the actuator at the top, at the predicted linear elastic limit of the system.

Table 1. Comparison of results at theoretical elastic limit of hinge			
	Small Angle Approx (Eq 4)	General Case (Eq 16)	% Error
Δ (in)	0.0102623	0.0102595	0.03%
δtop (in)	0.76032	0.76063	0.04 %
P (lb)	1418.85	1418.48	0.03 %

The assumption was therefore justified for the range of motion considered in this particular experiment.

Experimental Protocol

During testing of the structure, the actuator followed a quasi-static cyclic deflection pattern. The pattern ran for 12 cycles of increasing amplitude, with a

maximum displacement of .185 inches from equilibrium. The test protocol ran approximately 125 seconds at speeds low enough to make dynamic forces negligible. Due to the limited moment capacity of the load cell at the bottom of the setup, the plastic limit of the hinge could not be reached and the fuse-bars remained elastic.
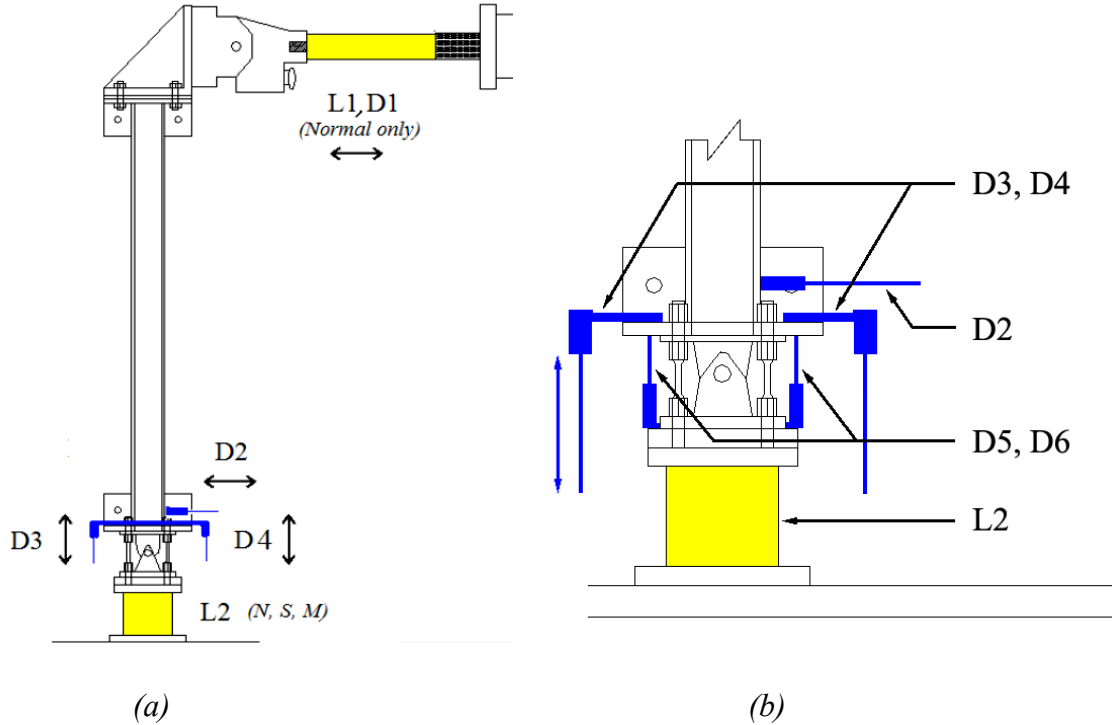

(a)   *(b)*

Figure 9: (a) Overall experimental setup and gauge placement; (b) Instrumentation

Initial Instrumentation

For all testing, the deflection (D1) and load (L1) imposed by the actuator was measured by gauges within the actuator arm itself. The overall stiffness of the system could be calculated using these two experimental values. The initial instrumentation for the hinge setup used two vertical displacement gauges (D3 and D4), one on either side of the hinge, as shown in Figure 9(a). This allowed the derivation of the rotation θ at the top of the hinge according to:

$$\theta = \arctan\left(\frac{D3+D4}{x}\right) \qquad\qquad \text{Eq. (17)}$$

where D3 and D4 = absolute displacement measurements (referenced to the reaction frame) and x = distance between these gauges. A third displacement gauge measuring lateral displacement (D2) was placed on top of the hinge. Using these two parameters, the resulting displacement at the top of the column due to movement of the hinge could be calculated by:

$$\delta_\theta = \theta \times L + D2 \qquad\qquad \text{Eq. (18)}$$

This quantity could then be subtracted from the total displacement, allowing the flexural component of deflection, δ_{flex}, to be separately analyzed. Placed underneath the hinge

was another load cell measuring moment, shear and normal forces, but due to extraneous rotation in this load cell the data taken from it was distorted and not used in analysis.

Modified Instrumentation

Subsequent tests used additional gauges about the hinge to separate the movement of various components making up the base fixture. Two additional gauges, labeled D5/6 in Figure 9(b), measured the relative movement of the top and bottom plate of the plastic hinge, thereby completely isolating the hinge from any rotations originating elsewhere. The final test setup enlisted the use of the Krypton Coordinate Measurement System, a camera system capable of recording the three-dimensional motion of small LEDs fixed to the structure. Nine such LEDs were placed on the various connecting plates and load cell, allowing the movement of each individual component to be tracked separately.

Analysis of Initial Experiment

Initial results using data from the actuator (L1 and D1 on Figure 9) yielded an unexpectedly low overall stiffness when compared to analytical predictions. Looking at Figure 11, the rotational stiffness of the hinge was also much lower than predicted using the rotations given by gauges D3/4. The experimental flexural stiffness, however, came within 5% of the expected value, presented in Table 2. Evidently, the flexural model for the S3x5.7 member was adequate, but as shown in Figure 11 the top of the hinge was rotating about three times more than predicted, creating the large error seen in overall stiffness in Figure 10. Understanding the rotational behavior of the hinge required more data.
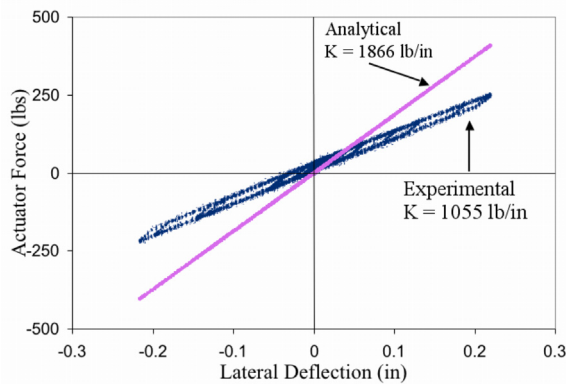

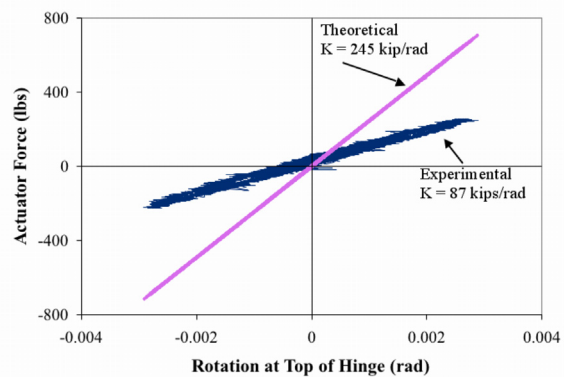*Figure 10: Total stiffness of entire setup*

Figure 11: Rotational stiffness of base (includes hinge and load cell)

Analysis of Modified Experiment

Using the data taken from gauges D5/6, the rotation of the hinge was separated from the motion of the remainder of the base. The true rotational stiffness of the hinge found using these gauges came within 5% of the originally predicted value, as shown below in Table 2. A comparison of the rotations taken from gauges D3/4 (magenta) and D5/6 (blue) shows an obvious discrepancy in Figure 12. These results clearly indicate that some other component was contributing to the rotation of the base, skewing results for the hinge and overall stiffness. Further separation of the motion in various components of the base was required to identify the source of this extra rotation.
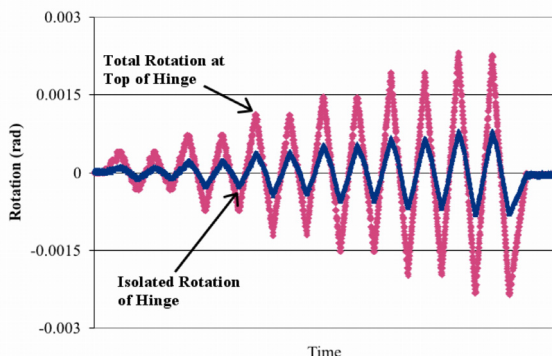

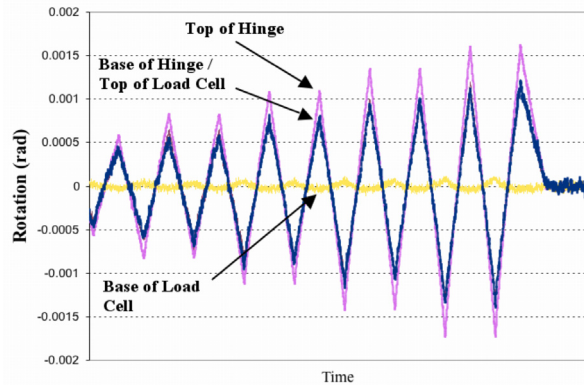*Figure 12: Rotational Comparison of Isolated Hinge and Top of Hinge*

Figure 13: Rotational Comparison of Top and Bottom of Load Cell and Hinge

With the use of the Krypton Coordinate Measurement System, the motion of each connecting element was recorded and used to derive the rotation of each element in the base structure. A comparison of the increasing rotation as one moves up from the reaction frame to the top of the hinge is shown in Figure 13. The considerable change in amplitude between the base and top of the load cell indicates that flexure of part or all of this load cell was the source of extraneous rotation skewing the total rotation at the top of the hinge.

Table 2. Comparison of analytical and initial experimental results			
	Analytical Result	Experimental Result	% Error
Rotational Stiffness	245 (kips/rad)	233 (kips/rad)	4.9 %
Flexural Stiffness	2930 (lb/in)	2800 (lb/in)	4.4 %

Energy Dissipation

Despite the absence of yielding in the fuse-bars, hysteresis was present during the loading cycles of the actuator, as shown in Figure 14. It is apparent that some component in the setup was yielding or slipping in a regular fashion, causing a transient behavior as the actuator switched direction of motion. Due to the numerous interfaces bolted together, the location of this component could not be determined. Figure 15 presents the

net work done on the column due to this phenomena, equivalent to the area within the hysteresis loop. In order to accurately analyze the energy dissipated by plastic hinge action, this work would have to be subtracted from the total work done on the column. It is desirable to stop this additional energy absorption since the component in question may weaken and fail after repeated cycles. Only the fuse-bars were intended to wear out and be replaced.
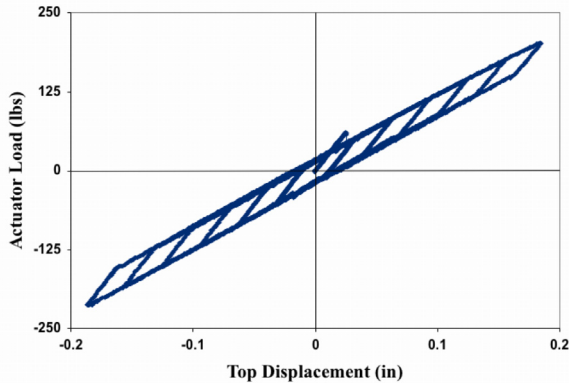

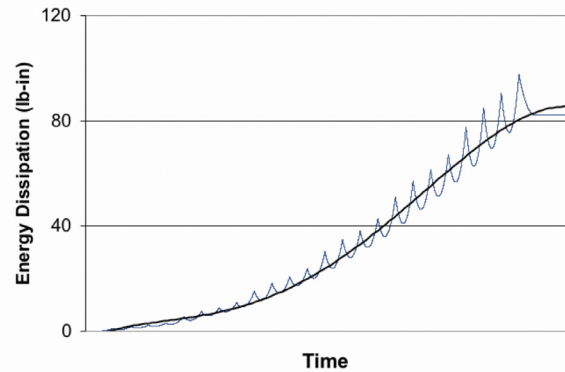Figure 14: Total stiffness, shown with hysteresis

Figure 15: Work done due to hysteresis

Conclusions:

Through experimental and analytical processes, an accurate model was developed for this hinge-column system within the elastic range of the fuse bars. In order for this hinge to be effectively used as an energy-dampening device, several design considerations must be investigated:
1. The moment capacity of the hinge, determined by the position, axial and bending stiffness, and yielding strength of the fuse bars, must be lower than that of the column.
2. The effective length of the fuse-bars can vary depending on direction of motion. Careful consideration of the manner in which the fuse bars are attached to the hinge is imperative.
3. The amount of deflection required to yield the hinge depends on the total stiffness of the system. This can be calculated by a series summation of the rotational stiffness of the hinge and the flexural stiffness of the column. As shown in this study, extraneous motion in the setup can greatly alter the total stiffness and must be taken into account for accurate predictions of deflection-controlled behavior.

Future Research:

Based on the results and methods used in this study, further analytical and experimental investigations of the following topics are suggested in order to more fully understand the setup:

1. Compression and tension tests of the hinge separate from the remainder of the setup could directly determine the effective length of the fuse bars, allowing for further verification of the analytical model for the hinge.
2. The hysteresis shown in the graphs above requires further investigation to determine the location of the yielding or slipping component. This may be achieved by use of the Krypton system.
3. In order to complete the model of the hinge, investigation of the plastic behavior of fuse bars must be made.

References

Cheng TC, Mander JB (1997): Seismic design of bridge columns based on control and repairability of damage. *Technical Report NCEER-97-0013*, Multidisciplinary Center for Earthquake Engineering Research, Buffalo, NY.